

Insensitive edge solitons in non-Hermitian topological lattices

Bertin Many Manda* and Vassos Achilleos†

Laboratoire d'Acoustique de l'Université du Mans (LAUM),
UMR 6613, Institut d'Acoustique - Graduate School (IA-GS), CNRS,
Le Mans Université, Av. Olivier Messiaen, 72085 Le Mans, France

In this work, we demonstrate that the synergetic interplay of topology, nonreciprocity and nonlinearity is capable of unprecedented effects. We focus on a nonreciprocal variant of the Su-Shrieffer-Heeger chain with local Kerr nonlinearity. We find a continuous family of non-reciprocal edge solitons (NESs) emerging from the topological edge mode, with near-zero energy, in great contrast from their reciprocal counterparts. Analytical results show that this energy decays exponentially towards zero when increasing the lattice size. Consequently, despite the absence of chiral symmetry within the system, we obtain zero-energy NESs, which are insensitive to growing Kerr nonlinearity. Even more surprising, these zero-energy NESs also persist in the strong nonlinear limit. Our work may enable new avenues for the control of nonlinear topological waves without requiring the addition of complex chiral-preserving nonlinearities.

During the last two decades, great progress has been achieved in understanding topological systems [1–9]. The promise is the developments of technological devices exploiting localized edge waves immune to fluctuations and defects. The manifestations of these topological edge modes (TMs) were observed in experiments in photonic [4, 10–12], atomic [13, 14], electronic [15, 16] and phononic [17–20] devices. Another domain which has been extensively debated recently are linear waves in non-Hermitian (NH) media [21]. These media offer promising solutions in implementing unidirectional, broadband waveguides and amplifiers [22], known to host a plethora of new phenomena like non-Hermitian skin effect (NHSE) [23, 24], complex-frequency and exceptional points [25]. In most cases, the NHSE originates from the asymmetry between the couplings which constraints most of the system normal modes (NMs) to be localized on a single interface of the system. This phenomenon has been experimentally demonstrated in photonics [26, 27], electronics [28], acoustics [29, 30] and mechanics [31–33]. Owing to this, it was shown that NHSE and TM can interact, leading to unprecedented level of manipulation of the latter, e.g., in phononic [32–35] and electric [36] systems.

Interestingly, the inclusion of nonlinear features in NH topological insulators has recently seen growing interest. Exciting developments like nonlinear NHSE [37–40], nonlinearly induced NH phase transitions [41] and nonlinear wave acceleration [42] have already been demonstrated. Furthermore, experiments featuring nonreciprocity revealed the realization of lossless unidirectional waveguides [42–45]. Following these efforts, we raise the question of what is the fate of nonlinear topological solitons (or breathers) [46–54] in the presence of nonreciprocity? Assuming that nonlinearity is perturbative, we can prematurely collect some elements of answers. Indeed, it was demonstrated [55, 56] that NH topological systems are exponentially sensitive to perturbations at the boundaries.

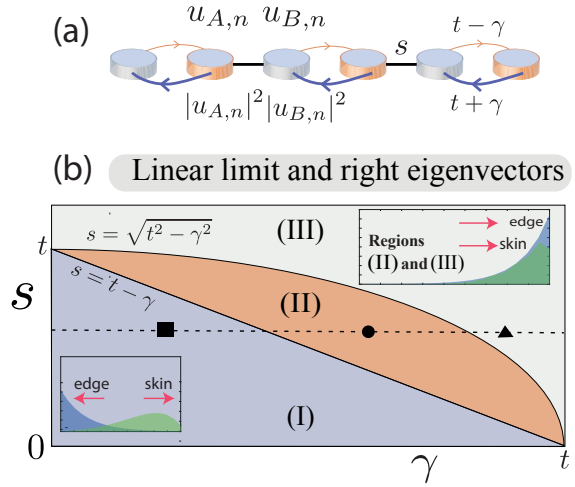


FIG. 1. (a): The nonreciprocal SSH model considered in this work with Kerr nonlinearity. (b) Phase diagram (γ, s) of the linearized model. The insets indicate the localization of the right TM and SMs.

Here we demonstrate an unanticipated insensitivity of the energy of nonlinear edge modes, which we hereby call nonreciprocal edge solitons (NES) as their intensity increases. We consider a Su-Shrieffer-Heeger (SSH) chain [57] with nonreciprocal couplings featuring Kerr nonlinearity. As we will explain below, this rather generic model exhibits a region in its parameter space whereby increasing the intensity, I , the energy, E , of the NES remains practically constant and exponentially decays toward $E = 0$, with growing lattice size N ,

$$\mathcal{S}_E = \frac{\partial E}{\partial I} \sim \exp(-\alpha_E N). \quad (1)$$

Our results are based on finite lattices whose governing equations read

$$\begin{aligned} E u_{A,n} &= (t + \gamma) u_{B,n-1} + s u_{B,n} + \sigma |u_{A,n}|^2 u_{A,n}, \\ E u_{B,n} &= s u_{A,n} + (t - \gamma) u_{A,n+1} + \sigma |u_{B,n}|^2 u_{B,n} \end{aligned}, \quad (2)$$

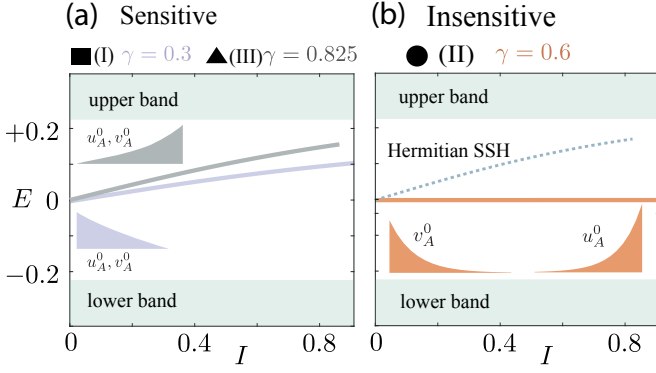


FIG. 2. The numerically obtained E of the NES against I , (a) for regions (I) and (III) and (b) for (II) with $\gamma = 0.3$, 0.825 and 0.6 respectively. The dashed lines in panel (b) show the corresponding Hermitian SSH model ($\gamma = 0$) for comparison [60]. The insets depict the localization sides of the TMs.

where E is the energy, $\sigma = \pm 1$ the nonlinear coefficient, s and $t \pm \gamma$ the positive nearest-neighbour couplings, and $\gamma > 0$ quantifies the strength of nonreciprocity. Here $u_{a,n}$ is the amplitude at cell with index n and sublattice $a = \{A, B\}$. In the linear limit, $|u_{a,n}|^2 \rightarrow 0$, Eq (2), reduces to a linear eigenvalue problem $H\vec{u} = E\vec{u}$, with the H being a non-Hermitian and chiral matrix [58]. Hereafter, we consider a chain of N cells with $2N - 1$ sites and open boundary conditions. The chirality ensures all bulk eigenenergies to come in pairs $E_k = \pm \sqrt{s^2 + \tilde{t}^2 + 2s\tilde{t} \cos(\frac{k\pi}{2N})}$ with $|k| = 1, 2, \dots, N-1$ and $\tilde{t} = \sqrt{t^2 - \gamma^2}$. Regarding their associated NMs, the non-Hermiticity implies the k -th right and left NMs, respectively \vec{u}_k and \vec{v}_k to be in general different [59]. Furthermore, these NMs are *skin* modes (SMs) satisfying $u_{k,a,n} \sim \beta^{(n-1)/2}$ and $v_{k,a,n} \sim \beta^{-(n-1)/2}$ with $\beta = (t + \gamma)/(t - \gamma)$ quantifying their localization [58]. As such, the right SMs are always localized on the left boundary, while the left ones are localized on the right sides of the chain, Fig. 1(b).

In addition, the choice of $2N - 1$ sites and chiral symmetry guarantee the presence of a NM with $E_0 = 0$, pinned as TM. It has zero support on the B-sublattice, $u_{0,B,n} = v_{0,B,n} = 0$, while the A-sublattice A satisfies

$$u_{0,A,n} = r_R^{n-1}, \quad v_{0,A,n} = r_L^{n-1}, \quad (3)$$

where $r_R = -s/(t - \gamma)$ and $r_L = -s/(t + \gamma)$. The localization of the TM is distinct from the SMs and can be used to identify three different regions, namely:

$$\begin{aligned} \text{(I):} & \quad s + \gamma < t, \quad |r_R|, |r_L| < 1, \\ \text{(II):} & \quad \sqrt{s^2 + \gamma^2} < t < s + \gamma, \quad |r_R| > 1, |r_L| < 1, \\ \text{(III):} & \quad \sqrt{s^2 + \gamma^2} > t, \quad |r_R|, |r_L| > 1. \end{aligned} \quad (4)$$

as highlighted in Fig. 1(b). In region (I) both the right and left TMs, are localised on the opposite side compared

to right SMs. On the other hand, for region (III) the nonreciprocity is dominating. It follows that the right and left TMs are opposite, and on the same side as their respective SMs with similar localization. Finally region (II) looks like (III) with the difference being the TMs and SMs exhibit distinct localization (see also Ref. [61]).

We now numerically calculate the nonlinear solutions of Eqs. (2) stemming from the TM, using a pseudo-arclength solver [62–64] and follow families of solutions of increasing intensity, i.e. $I = \sum_l |u_l|^2$. The solver returns both the E and the $u_{a,n}$ of the obtained solutions. Figure 2(a) shows the dependence of E as a function of I for representative cases of the found families of NESs on a chain of $N = 17$ with $\gamma = 0.3$ and 0.825 ($s = 0.6$) in regions (I) and (III) respectively. It depicts a behavior similar to the Hermitian SSH model with $\gamma = 0$ [see dashed curve in Fig. 2(b)]. That is to say, the energy departs from the origin, growing with increasing intensity till approaching the linear upper band for $\sigma > 0$. This behaviors is associated to the chiral symmetry breaking induced by Kerr nonlinearity which do not guarantee the presence of modes at $E = 0$.

An unexpected result is found in region (II). Indeed, despite the aforementioned chiral symmetry breaking we find the family above has $E \approx 0$ when increasing the amplitude, as shown in case of $\gamma = 0.6$ and $s = 0.6$ in Fig. 2(b). In order to explain the origin of this behavior, we rely on the perturbation theory, assuming small amplitude nonlinear solutions originating from the k -th NM expand as $\vec{u}_k = \vec{u}_k^0 + \epsilon \vec{u}_k^1 + \mathcal{O}(\epsilon^2)$ with the energy given by $E_k = E_k^0 + \epsilon E_k^1 + \mathcal{O}(\epsilon^2)$. Here the ϵ controls the amplitude and the (\vec{u}_k^0, E_k^0) are retrieved resolving the linearized limit. The details of the first order perturbation analysis (\vec{u}_k^1, E_k^1) can be found in the supplementary [58]. Consequently, we define the rate of change of the energy to the intensity referred to as energy sensitivity factor,

$$\mathcal{S}_E^k = \frac{\partial E_k}{\partial I} \approx \rho_k E_k^1(\sigma), \quad (5)$$

where $\rho_k^{-1} = \vec{u}_k^{0,T} \vec{u}_k^0$ is analogous to the Petermann factor [65]. One of the main results of our work is the following relation unique to the NES:

$$\mathcal{S}_E^0 = S_0 \frac{(r_L r_R r_R r_R)^N - 1}{[(r_R r_R)^N - 1] [(r_L r_R)^N - 1]}, \quad (6)$$

with S_0 being a positive nonzero constant [58]. This expression implies that the energy shift of the NES is obtained solely by examining the right and left TMs. Thus, using Eqs. (4) and (6), we can predict behavior of the families of NESs emerging from the TM within the parameter space of the linearized model, Fig. 1(b). More specifically; for sufficiently large N values; we find that in regions (I) and (III) the $\mathcal{S}_E^0 \sim 1$. Thus a similar energy grows against the intensity must be observed for all N ,

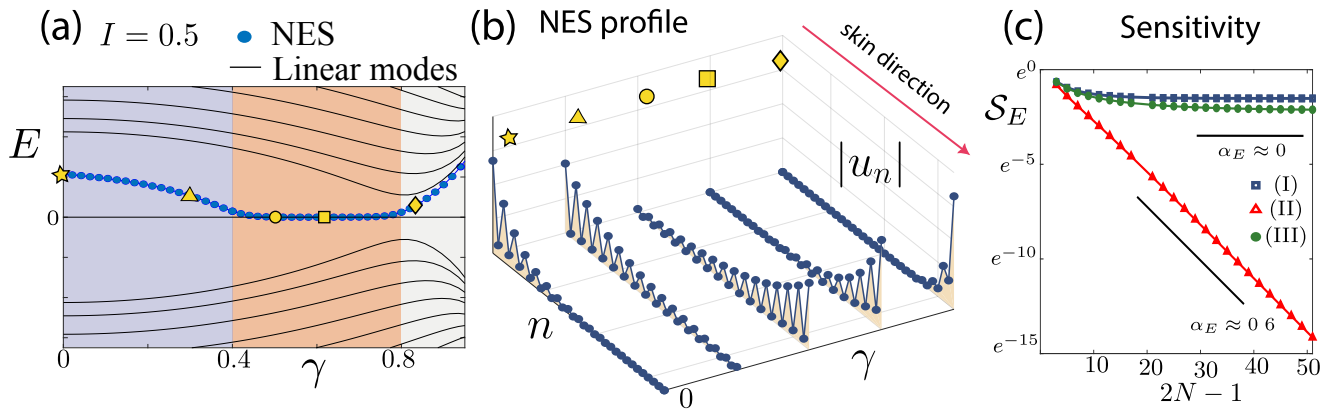


FIG. 3. (a) Dependence of the energy of the NESs at $I = 0.5$ against γ with $s = 0.6$. The black lines are the spectrum of the linearized limit. (b) Representative cases of NESs for the Hermitian ($\gamma = 0$) and NH SSH chains with $\gamma = 0.3, 0.5$ and 0.6 and 0.825 respectively the star, triangle, circle, square and diamond dots. (c) Energy sensitivity of the NESs as function of the lattice size for (I) $\gamma = 0.3$, (II) 0.6 and (III) 0.825 .

confirming the results of Fig. 2(a). On the other hand, in region (II) we obtain $\mathcal{S}_E^0 \sim (r_L r_R)^N$. It follows rewriting $r_L r_R = e^{-\alpha_E}$ with $0 < \alpha_E(r_R, r_L) < 1$, that the energy sensitivity is exponentially decaying with N . As such, for large lattices we obtain zero-energy NESs, explaining the unexpected numerical observation of Fig. 2(b).

We scan the system's parameter space in Fig. 1(b), performing numerical continuation on a chain of $N = 17$ at fixed nonlinearity, $I = 0.5$, varying the γ along the section $s = 0.6$. Along this line, the $\gamma = 0.4$ delimits regions (I) and (II) and $\gamma = 0.8$, regions (II) and (III). The results are shown in Fig. 3(a). Clearly at $\gamma = 0$ in the Hermitian case, an energy shift away from $E = 0$ is seen [star dot]. As $\gamma \rightarrow 0.4$ this energy shift remains non-trivial, while tending to decrease with increasing values of γ across region (I). Representative NESs of this region are also shown in Fig. 3(b) for $\gamma = 0$ and 0.3 respectively the star and triangle dots. These NESs stay localized at the same side as their TM, yet developing support also on the B -sublattice. In addition, similar results are also seen for region (III) where $\gamma > 0.8$ [Fig. 3(a)], with a representative NES depicted by the diamond dot in Fig. 3(b). These observations, once again, are due to the chiral symmetry breaking owing to the Kerr nonlinearity.

Bearing the above in mind, entering region (II) with $0.4 < \gamma < 0.8$, we find this family of NESs at $I = 0.5$ has $E \approx 0$, Fig. 3(a). In addition, we depict representative NESs with $\gamma = 0.5$ and 0.6 respectively the circle and square dots in Fig. 3(b). Their profiles clearly show localized shapes, with support also on the B -sublattice.

Figure 3(c) displays the dependence of the sensitivity factor, \mathcal{S}_E^0 against the lattice size N . The measures are obtained as in Fig. 3(a) for representative parameter sets (I) $\gamma = 0.3$, (II) 0.6 and (III) 0.825 with $s = 0.6$. For regions (I) and (III), a clear saturation of the \mathcal{S}_E^0 to values in the interval $[0.1, 1]$ is seen. On the other hand, for

$\gamma = 0.6$ in region (II), we find an exponentially decaying sensitivity factor, $\mathcal{S}_E^0 \sim e^{-0.6N}$. It is worth emphasizing that we have also checked that this insensitivity of the NESs does not hold for the nonlinear SMs and are robust whilst the addition of disorder [58].

Let us now focus on the shape of the NES rather than its energy. The perturbation theory can also be used to define the wavefunction sensitivity

$$\mathcal{S}_{\vec{u}}^k = \frac{\partial \vec{u}_k}{\partial I} \approx \rho_k V_k^1(\sigma), \quad (7)$$

with $V_k^1 = |\sum_{l \neq k} C_l^1(\sigma) u_l^0|$ being a mode overlap integral [58]. Consequently, the $\mathcal{S}_{\vec{u}}^0$ quantifies how strong the TM couples to the SMs when increasing the intensity [58]. We project the NESs of Fig. 3(b) onto the NM basis, $\vec{u} = \sum_k C_k \vec{u}_k^0$. The $|C_k|$, are shown in Fig. 4(a). It follows that despite these NESs being obtained for the same nonlinearity, $I = 0.5$, the TM strongly couples with the SMs [star, rectangle and diamond dots] in regions (I) and (III), while in region (II), this coupling is smaller [circle and square dots]. Further, the dependence of $\mathcal{S}_{\vec{u}}^0$ as function of N shows that this mode couplings growth or remains constant with increasing N in regions (I) and (III) respectively. Indeed, we expect that as the lattice size grows, the number of NMs the TM pairs with increases. Remarkably, region (II), evades this anticipation and the $\mathcal{S}_{\vec{u}}^0$ tends to exponentially vanish. In the supplementary [58], we shows that these results are independent of I . We also demonstrate that, similar to the TM case, the shape of finite amplitude NESs can be modified by tuning γ (see also [33]).

With respect to the linear stability of the NESs, the latter is obtained monitoring a small deviation $\chi w_{a,n}(\tau = 0)$ from the NES $u_{a,n}$ of the form $\psi_{a,n} = (u_{a,n} + \chi w_{a,n}) e^{iE\tau}$ with $\chi \ll 1$ and τ being the temporal variable [66]. Considering $w_{a,n} \sim e^{i\lambda\tau}$ leads to a linear eigenvalue problem $\lambda \vec{w} = Z \vec{w}$ [58]. Thus, instabil-

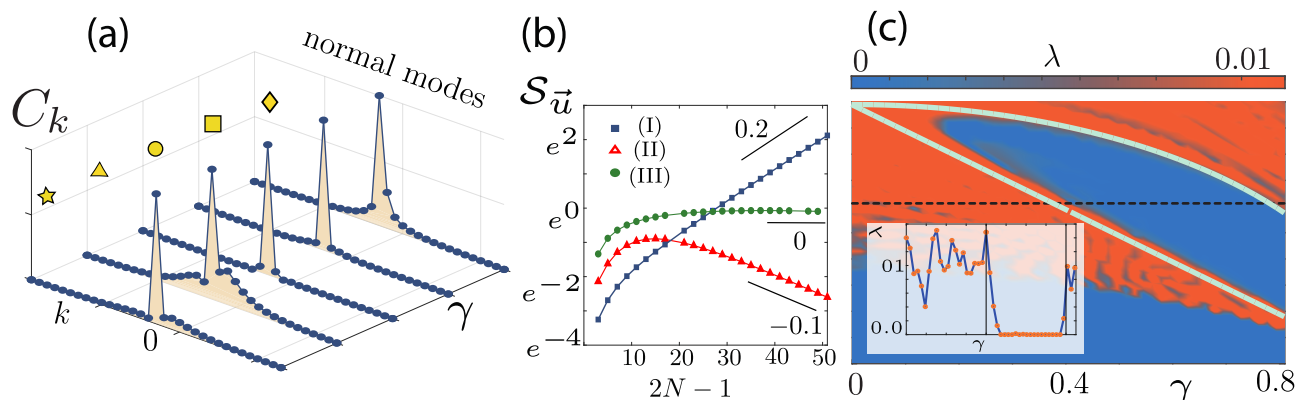


FIG. 4. (a) Projection, C_k , of the NESs in Fig. 3(b) into the NMs. The $|C_k|$ are rescaled by their maximum for clarity. (b) Similar to Fig. 3(c) but for the wavefunction's sensitivity. (c) Stability of the NES at fixed $I = 0.5$, across the phase diagram of Fig. 1(b). We display the largest eigenvalue, λ , of the stability matrix [58]. The white line and curve represent $s = t - \gamma$ and $s^2 = t^2 - \gamma^2$ respectively. Inset: Dependence of λ against γ at $s = 0.6$ (see dashed line).

ities are signaled by the imaginary part of λ . The largest value of the imaginary part of λ is plotted in Fig. 4(c), for the parameter space of Fig. 1(b) using the same setting as in Fig. 3. We observe two regions of stable NESs [blue islands]. The stability in the lower islands, is likely due to large band gap, as $s \rightarrow 0$. On the other hand, despite region (II), being in the neighbourhood of the band closing the obtained NESs are in general linearly stable, see also inset of Fig. 4(c).

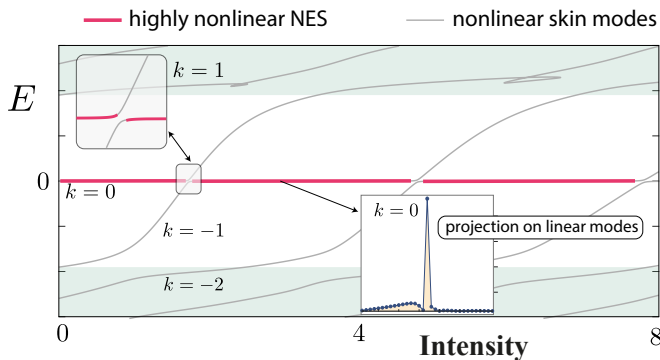


FIG. 5. The energy, E against intensity, I for the families of nonlinear modes emerging from the NMs [we show 8 of them] on a chain of $N = 17$ cells with (II) $\gamma = 0.6$ and $s = 0.6$. The insets (left) zoom into a transition and (right) depict the projection of the NES of $E \approx 0$ at $I = 2.75$ into the NMs basis (red dots).

Finally, we present results beyond the weakly nonlinear regime and its perturbative analysis. To do so we perform numerical continuation like in Fig. 2 for all NMs with $\gamma = 0.6$ and $s = 0.6$, in region (II), toward $I \rightarrow \infty$. The results are shown in Fig. 5. It displays persistent NESs with $E \approx 0$ (red lines) even at large intensity. In fact, we see that as we increases the nonlinearity from $I = 0$, the families of NESs originating from the TM ($k = 0$) at

constant $E \approx 0$, and the one emerging from the SM with $k = -1$ (grey line) of growing E , inexorably comes closes around $I = 2.5$ without crossing. We find at this point the characters of the two families are exchanged [left inset of Fig. 5]. Consequently, the family of NESs emerging from the $k = -1$ SM has constants $E \approx 0$ for growing I pass $I = 2.5$. Further, we project on the NM basis the high-amplitude NES at $I = 2.75$ and find weak couplings of the TM with its surrounding, like what is seen for weak amplitude NESs, right-inset of Fig. 5. Furthermore, we find a cascade of such transitions between the consecutive families of nonlinear modes emerging from the SMs with $k = -1$ and -2 , $k = -2$ and -3 , etc.

In summary, we have investigated the spectral sensitivity of edge solitons arising from the topological modes within a nonreciprocal Su-Schrieffer-Heeger chain featuring local Kerr nonlinearity. We found in large enough lattices, such a family of nonreciprocal non-edge solitons (NESs) with zero-energy without requiring chiral symmetry, as usually the case [54], for e.g., when implementing complex nonlinear couplings [16, 67]. Furthermore, we anticipate that our findings can be extended to other classes of nonlinear localized modes, such as breathers [68, 69]. Consequently, our work may open new ways to manipulate waves in topological systems for applications in sensing, lasing and information processing.

V.A and B.M.M acknowledge the support of the program *Etoiles Montantes en Pays de la Loire* and the EU H2020 ERC StG “NASA” Grant Agreement No. 101077954.

* bertin.many_manda@univ-lemans.fr

† achilleos.vassos@univ-lemans.fr

[1] M. Z. Hasan and C. L. Kane, Colloquium: Topological

- insulators, *Rev. Mod. Phys.* **82**, 3045 (2010).
- [2] I. Mondragon-Shem, T. L. Hughes, J. Song, and E. Prodan, Topological criticality in the chiral-symmetric AIII class at strong disorder, *Phys. Rev. Lett.* **113**, 046802 (2014).
- [3] G. Ma, M. Xiao, and C. T. Chan, Topological phases in acoustic and mechanical systems, *Nat. Rev. Phys.* **1**, 281 (2019).
- [4] T. Ozawa, H. M. Price, A. Amo, N. Goldman, M. Hafezi, L. Lu, M. C. Rechtsman, D. Schuster, J. Simon, O. Zilberberg, and I. Carusotto, Topological photonics, *Rev. Mod. Phys.* **91**, 015006 (2019).
- [5] L. J. Maczewsky, M. Heinrich, M. Kremer, S. K. Ivanov, M. Ehrhardt, F. Martinez, Y. V. Kartashov, V. V. Konotop, L. Torner, D. Bauer, and A. Szameit, Nonlinearity-induced photonic topological insulator, *Science* **370**, 701 (2020).
- [6] H. Nassar, B. Yousefzadeh, R. Fleury, M. Ruzzene, A. Alù, C. Daraio, A. N. Norris, G. Huang, and M. R. Haberman, Nonreciprocity in acoustic and elastic materials, *Nature Reviews Materials* **5**, 667 (2020).
- [7] M. Segev and M. A. Bandres, Topological photonics: Where do we go from here?, *Nanophotonics* **10**, 425 (2021).
- [8] X. Zhang, F. Zangeneh-Nejad, Z.-G. Chen, M.-H. Lu, and J. Christensen, A second wave of topological phenomena in photonics and acoustics, *Nature* **618**, 687 (2023).
- [9] S. Coen, B. Garbin, G. Xu, L. Quinn, N. Goldman, G.-L. Oppo, M. Erkintalo, S. G. Murdoch, and J. Fatome, Nonlinear topological symmetry protection in a dissipative system, *Nature Communications* **15**, 1398 (2024).
- [10] D. Smirnova, D. Leykam, Y. Chong, and Y. Kivshar, Nonlinear topological photonics, *Applied Physics Reviews* **7**, 021306 (2020).
- [11] C. Jörg, M. Jürgensen, S. Mukherjee, and M. C. Rechtsman, Optical control of topological end states via soliton formation in a 1D lattice, arXiv preprint arXiv:2404.09560 (2024).
- [12] A. Szameit and M. C. Rechtsman, Discrete nonlinear topological photonics, *Nature Physics* , 1 (2024).
- [13] E. J. Meier, F. Alex An, A. Dauphin, M. Maffei, P. Massignan, T. L. Hughes, and B. Gadway, Observation of the topological Anderson insulator in disordered atomic wires, *Science* **362**, 929 (2018).
- [14] E. Lustig, S. Weimann, Y. Plotnik, Y. Lumer, M. A. Bandres, A. Szameit, and M. Segev, Photonic topological insulator in synthetic dimensions, *Nature* **567**, 356 (2019).
- [15] J. Dong, V. Juričić, and B. Roy, Topoelectric circuits: Theory and construction, *Phys. Rev. Res.* **3**, 023056 (2021).
- [16] X. Guo, L. Jezequel, M. Padlewski, H. Lissek, P. Delplace, and R. Fleury, Practical realization of chiral nonlinearity for strong topological protection (2024), arXiv:2403.10590 [cond-mat.mes-hall].
- [17] L. Xin, Y. Siyuan, L. Harry, L. Minghui, and C. Yanfeng, Topological mechanical metamaterials: A brief review, *Current Opinion in Solid State and Materials Science* **24**, 100853 (2020).
- [18] S. Zheng, G. Duan, and B. Xia, Progress in topological mechanics, *Applied Sciences* **12**, 10.3390/app12041987 (2022).
- [19] Y. Betancur-Ocampo, B. Manjarrez-Montañez, A. M. Martínez-Argüello, and R. A. Méndez-Sánchez, Twofold topological phase transitions induced by third-nearest-neighbor hoppings in one-dimensional chains, *Phys. Rev. B* **109**, 104111 (2024).
- [20] T. Lee, B. Many Manda, X. Li, Z. Yu, G. Theocharis, and C. Daraio, Control of multimodal topological edge modes in magnetoelastic lattices, *Phys. Rev. Appl.* **21**, 024049 (2024).
- [21] L. Sirota, R. Ilan, Y. Shokef, and Y. Lahini, Non-Newtonian topological mechanical metamaterials using feedback control, *Phys. Rev. Lett.* **125**, 256802 (2020).
- [22] M. Brandenbourger, X. Locsin, E. Lerner, and C. Coulais, Non-reciprocal robotic metamaterials, *Nature communications* **10**, 4608 (2019).
- [23] N. Okuma, K. Kawabata, K. Shiozaki, and M. Sato, Topological origin of non-Hermitian skin effects, *Phys. Rev. Lett.* **124**, 086801 (2020).
- [24] Q. Liang, D. Xie, Z. Dong, H. Li, H. Li, B. Gadway, W. Yi, and B. Yan, Dynamic signatures of non-Hermitian skin effect and topology in ultracold atoms, *Phys. Rev. Lett.* **129**, 070401 (2022).
- [25] H. Meng, Y. S. Ang, and C. H. Lee, Exceptional points in non-Hermitian systems: Applications and recent developments, *Applied Physics Letters* **124**, 060502 (2024).
- [26] S. Weidemann, M. Kremer, T. Helbig, T. Hofmann, A. Stegmaier, M. Greiter, R. Thomale, and A. Szameit, Topological funneling of light, *Science* **368**, 311 (2020).
- [27] Q. Lin, T. Li, L. Xiao, K. Wang, W. Yi, and P. Xue, Observation of non-Hermitian topological Anderson insulator in quantum dynamics, *Nature Communications* **13**, 3229 (2022).
- [28] S. Liu, R. Shao, S. Ma, L. Zhang, O. You, H. Wu, Y. Jiang Xiang, T. Jun Cui, and S. Zhang, Non-Hermitian skin effect in a non-Hermitian electrical circuit, *Research* **2021**, 1 (2021).
- [29] L. Zhang, Y. Yang, Y. Ge, Y.-J. Guan, Q. Chen, Q. Yan, F. Chen, R. Xi, Y. Li, D. Jia, S.-Q. Yuan, H.-X. Sun, H. Chen, and B. Zhang, Acoustic non-Hermitian skin effect from twisted winding topology, *Nature communications* **12**, 6297 (2021).
- [30] A. Maddi, Y. Auregan, G. Penelet, V. Pagneux, and V. Achilleos, Exact analog of the Hatano-Nelson model in one-dimensional continuous nonreciprocal systems, *Phys. Rev. Res.* **6**, L012061 (2024).
- [31] M. Brandenbourger, X. Locsin, E. Lerner, and C. Coulais, Non-reciprocal robotic metamaterials, *Nature communications* **10**, 4608 (2019).
- [32] A. Ghatak, M. Brandenbourger, J. van Wezel, and C. Coulais, Observation of non-Hermitian topology and its bulk-edge correspondence in an active mechanical metamaterial, *Proceedings of the National Academy of Sciences* **117**, 29561 (2020).
- [33] W. Wang, X. Wang, and G. Ma, Non-Hermitian morphing of topological modes, *Nature* **608**, 50 (2022).
- [34] P. Gao, M. Willatzen, and J. Christensen, Anomalous topological edge states in non-Hermitian piezophononic media, *Phys. Rev. Lett.* **125**, 206402 (2020).
- [35] W. Zhu, W. X. Teo, L. Li, and J. Gong, Delocalization of topological edge states, *Phys. Rev. B* **103**, 195414 (2021).
- [36] Z. Lu, X. Chen, Y. Hu, J. Wu, J. Lu, X. Huang, W. Deng, and Z. Liu, Extended states isolated in the band gap in non-Hermitian electrical circuits, *Phys. Rev. Appl.* **21**, 034043 (2024).
- [37] C. Yuce, Nonlinear non-Hermitian skin effect, *Physics Letters A* **408**, 127484 (2021).

- [38] M. Ezawa, Dynamical nonlinear higher-order non-Hermitian skin effects and topological trap-skin phase, *Physical Review B* **105**, 125421 (2022).
- [39] H. Jiang, E. Cheng, Z. Zhou, and L.-J. Lang, Nonlinear perturbation of a high-order exceptional point: Skin discrete breathers and the hierarchical power-law scaling, *Chinese Physics B* **32**, 084203 (2023).
- [40] B. Many Manda, R. Carretero-González, P. G. Kevrekidis, and V. Achilleos, Skin modes in a nonlinear Hatano-Nelson model, *Phys. Rev. B* **109**, 094308 (2024).
- [41] T. Dai, Y. Ao, J. Mao, Y. Yang, Y. Zheng, C. Zhai, Y. Li, J. Yuan, B. Tang, Z. Li, J. Luo, W. Wang, X. Hu, Q. Gong, and J. Wang, Non-Hermitian topological phase transitions controlled by nonlinearity, *Nature Physics* **20**, 101 (2024).
- [42] J. Veenstra, O. Gamayun, X. Guo, A. Sarvi, C. V. Meinersen, and C. Coulais, Non-reciprocal topological solitons in active metamaterials, *Nature* **627**, 528 (2024).
- [43] H. Li and S. Wan, Dynamic skin effects in non-Hermitian systems, *Phys. Rev. B* **106**, L241112 (2022).
- [44] S. Jana and L. Sirota, Tunneling-like wave transmission in non-Hermitian lattices with mirrored nonreciprocity, *arXiv preprint arXiv:2312.16182* (2023).
- [45] Z. Li, L.-W. Wang, X. Wang, Z.-K. Lin, G. Ma, and J.-H. Jiang, Observation of dynamic non-Hermitian skin effects, *arXiv preprint arXiv:2312.07564* (2023).
- [46] M. J. Ablowitz, C. W. Curtis, and Y.-P. Ma, Linear and nonlinear traveling edge waves in optical honeycomb lattices, *Phys. Rev. A* **90**, 023813 (2014).
- [47] Y. Hadad, A. B. Khanikaev, and A. Alù, Self-induced topological transitions and edge states supported by nonlinear staggered potentials, *Phys. Rev. B* **93**, 155112 (2016).
- [48] D. Leykam and Y. D. Chong, Edge solitons in nonlinear-photonic topological insulators, *Physical Review Letters* **117**, 143901 (2016).
- [49] Y. Lumer, M. C. Rechtsman, Y. Plotnik, and M. Segev, Instability of bosonic topological edge states in the presence of interactions, *Phys. Rev. A* **94**, 021801 (2016).
- [50] R. K. Pal, J. Vila, M. Leamy, and M. Ruzzene, Amplitude-dependent topological edge states in nonlinear phononic lattices, *Phys. Rev. E* **97**, 032209 (2018).
- [51] R. Chaunsali and G. Theocharis, Self-induced topological transition in phononic crystals by nonlinearity management, *Phys. Rev. B* **100**, 014302 (2019).
- [52] R. Chaunsali, H. Xu, J. Yang, P. G. Kevrekidis, and G. Theocharis, Stability of topological edge states under strong nonlinear effects, *Phys. Rev. B* **103**, 024106 (2021).
- [53] Y.-P. Ma and H. Susanto, Topological edge solitons and their stability in a nonlinear Su-Schrieffer-Heeger model, *Phys. Rev. E* **104**, 054206 (2021).
- [54] L. Jezequel and P. Delplace, Nonlinear edge modes from topological one-dimensional lattices, *Phys. Rev. B* **105**, 035410 (2022).
- [55] J. C. Budich and E. J. Bergholtz, Non-Hermitian topological sensors, *Phys. Rev. Lett.* **125**, 180403 (2020).
- [56] H. Yuan, W. Zhang, Z. Zhou, W. Wang, N. Pan, Y. Feng, H. Sun, and X. Zhang, Non-Hermitian topoelectrical circuit sensor with high sensitivity, *Advanced Science* **10**, 2301128 (2023).
- [57] W. P. Su, J. R. Schrieffer, and A. J. Heeger, Solitons in polyacetylene, *Phys. Rev. Lett.* **42**, 1698 (1979).
- [58] See Supplemental Material at <http://link.journal.domain/supplemental/doi>, for additional information which includes Refs.[cite].
- [59] It follows that in the rest of this paper we use the biorthogonality relation: $\vec{v}_k^T \vec{u}_{k'} = \delta_{kk'}$.
- [60] The energies $E_{l-} < x < E_{l+}$ are rescaled as $y = (x - E_{l-})(E_{m+} - E_{m-}) / (E_{l+} - E_{l-}) + E_{m-}$. It follows that $E_{m-} < y < E_{m+}$. We apply this process each time we want two sets of parameters of the system to have the same width of the energy band gap.
- [61] J. Cheng, X. Zhang, M.-H. Lu, and Y.-F. Chen, Competition between band topology and non-Hermiticity, *Phys. Rev. B* **105**, 094103 (2022).
- [62] E. Doedel, H. B. Keller, and J. P. Kernevez, Numerical analysis and control of bifurcation problems (I): Bifurcation in finite dimensions, *International Journal of Bifurcation and Chaos* **01**, 493 (1991).
- [63] A. Dhooge, W. Govaerts, Y. A. Kuznetsov, H. G. Meijer, and B. Sautois, New features of the software MatCont for bifurcation analysis of dynamical systems, *Mathematical and Computer Modelling of Dynamical Systems* **14**, 147 (2008).
- [64] Openly accessible at: <https://sourceforge.net/projects/matcont/files/>.
- [65] J. Wiersig, Petermann factors and phase rigidities near exceptional points, *Phys. Rev. Res.* **5**, 033042 (2023).
- [66] D. Pelinovsky, P. Kevrekidis, and D. Frantzeskakis, Stability of discrete solitons in nonlinear Schrödinger lattices, *Physica D: Nonlinear Phenomena* **212**, 1 (2005).
- [67] K. Bai, J.-Z. Li, T.-R. Liu, L. Fang, D. Wan, and M. Xiao, Arbitrarily configurable nonlinear topological modes, *arXiv preprint arXiv:2402.07224* (2024).
- [68] S. Aubry, Breathers in nonlinear lattices: Existence, linear stability and quantization, *Physica D: Nonlinear Phenomena* **103**, 201 (1997).
- [69] S. Flach and A. V. Gorbach, Discrete breathers — Advances in theory and applications, *Physics Reports* **467**, 1 (2008).